Environmental Science and Pollution Research (2023) 30:59660–59675
https://doi.org/10.1007/s11356-023-26752-5

RESEARCH ARTICLE

Study on mutual harmless treatment of electrolytic manganese residue and red mud

Jing Zhang[1] · Rui Li[1] · Yu Zhang[1] · Weilong He[1] · Junjie Yang[1] · Yu Wang[1]

Received: 10 December 2022 / Accepted: 27 March 2023 / Published online: 4 April 2023

Abstract

Electrolytic manganese residue (EMR) and red mud (RM) are solid waste by-products of the metal manganese and alumina industries, respectively. Under long-term open storage, ammonia nitrogen and soluble manganese ions in EMR and alkaline substances in RM severely pollute and harm the environment. In order to alleviate the pollution problem of EMR and RM. In this study, the alkaline substances in RM were used to treat ammonia nitrogen and soluble manganese ions in EMR. The results confirm the following suitable treatment conditions for the mutual treatment of EMR and RM: EMR–RM mass ratio = 1:1, liquid–solid ratio = 1.4:1, and stirring time = 320 min. Under these conditions, the elimination ratios of ammonia nitrogen (emitted in the form of ammonia gas) and soluble manganese ions (solidified in the form of $Mn_{3.88}O_7(OH)$ and KMn_8O_{16}) are 85.87 and 86.63%, respectively. Moreover, the alkaline substances in RM are converted into neutral salts (Na_2SO_4 and $Mg_3O(CO_3)_2$), achieving de-alkalinisation. The treatment method can also solidify the heavy metal ions—Cr^{3+}, Cu^{2+}, Ni^{2+}, and Zn^{2+}—present in the waste residue with leaching concentrations of 1.45 mg/L, 0.099 mg/L, 0.294 mg/L, and 0.449 mg/L, respectively. This satisfies the requirements of the Chinese standard GB5085.3–2007. In the mutual treatment of EMR and RM, the kinetics of ammonia nitrogen removal and manganese-ion solidification reactions are controlled via a combination of membrane diffusion and chemical reaction mechanisms.

Keywords Electrolytic manganese residue · Red mud · Harmless treatment · Heavy metal solidification

Introduction

EMR is a solid waste produced by manganese metal production (electrolytic production process) (Zhang and Cheng 2007). For every 1 ton of metal manganese produced, 10–12 tons of EMR is by-produced (Tian et al. 2019; Li et al. 2015). Currently, the main treatment method of EMR is open storage. In China, the stock of EMR has exceeded 150 million tons (Shu et al. 2020a, b). The main components of EMR are gypsum, quartz, alumina, and iron oxide. Additionally, it also contains a small amount of harmful substances such as ammonia nitrogen and soluble manganese ions (Duan et al. 2021; Shu et al. 2017). In long-term open storage, the ammonia nitrogen and soluble manganese ions in EMR will leach into the ground owing to rainwater immersion, which seriously pollutes the surrounding soil and water sources (Duan et al. 2010; Qian et al. 2012; Chen et al. 2016; He et al. 2021b; Huang and Zhang 2022). To alleviate the pollution problems caused by EMR, harmless treatment of EMR is imperative.

Red mud (RM) is a solid waste produced from alumina production (Klauber et al. 2011; Khairul et al. 2019; Patil and Thorat 2022). Currently, the main treatment measure for RM in industry is also open storage. In China, the stockpile of RM is also as high as 600 million tonnes (Liu et al. 2021). RM mainly comprises sodalite, nepheline, hematite, calcite, and alkaline substances (gibbsite, boehmite, and katoite). In the long-term open storage, the alkaline substances in RM will also leach out owing to rainwater immersion, causing

Responsible Editor: Weiming Zhang

Highlights
- Mutual treatment of electrolytic manganese residue and red mud is proposed.
- Achieve harmless discharge and storage of electrolytic manganese residue and red mud.
- Realise harmless pretreatment method of industrial hazardous waste at low cost.

✉ Yu Zhang
342114915@qq.com

[1] College of Chemistry and Chemical Engineering, Guizhou University, Guiyang 550025, Guizhou, China

damage to the surrounding ecological environment (Wang et al. 2018a; Winkler et al. 2018). Therefore, the dealkalisation of RM is also crucial.

Adding chemical reagents to transform and remove harmful substances is an effective method for harmless treatment of EMR and RM. For example, alkaline reagents such as NaOH, CaO, Na_3PO_4, and Na_2HPO_4 can be added to EMR for removing or solidifying ammonia and soluble manganese ions in EMR in the form of ammonia gas, $NH_4MgPO_4{\cdot}nH_2O$, $Mn(OH)_2$, MnO_2, MnOOH, and $Mn_3(PO_4)_2(OH)_4{\cdot}4H_2O$ to realise harmless treatment of EMR (Shu et al. 2016; Zhou et al. 2013; Deng et al. 2021). By using hydrochloric acid, sulphuric acid, or SO_2, CO_2 and other acidic gases to react with the alkaline substances in RM, the alkaline substances are converted into neutral salts such as chloride, sulphate, and carbonate (Luo et al. 2017; Hu et al. 2020). This treatment method is simple and effective, and its processing capacity is large. The core idea is to consume alkaline substances to remove and solidify ammonia nitrogen and soluble manganese ions. Therefore, alkaline substances such as gibbsite, boehmite, and katoite in RM may also have the feasibility of treating ammonia nitrogen and soluble manganese ions in EMR. At the same time, this process consumes the alkaline substances in RM, which also has the effect of treating the RM. Therefore, the mutual treatment of EMR and RM is a good approach to realise the simultaneous and harmless treatment of two solid wastes.

Based on this, EMR and RM were used for mutual harmless treatment in this study. Suitable treatment conditions for the mutual harmless treatment of EMR and RM. The material composition changes, reaction mechanism, and kinetic mechanism of the system were studied. After treatment, the material composition, microstructure, and heavy metal leaching behaviour of the mixed residue were analysed. Determine the practical feasibility of mutual harmless treatment of EMR and RM. This study can also provide guidance for the mutual harmless treatment of EMR, RM, and other wastes.

Materials and methods

Materials

The solid wastes used in this study were EMR and RM. EMR (pH = 6.5) was sourced from a metal manganese industry factory in Dalong Town, Tongren City, Guizhou Province, China. RM (pH = 9.73) was sourced from an alumina industry factory in the same city (Bayer RM). EMR and RM were dried (80 ℃) and ground to a particle size of less than 200 mesh. The analytically pure chemical reagents used in this study were sodium hydroxide, mercury iodide, potassium iodide, potassium periodate, nitric acid, potassium pyrophosphate, and sodium acetate trihydrate. These reagents were purchased from Tianjin Zhiyuan Chemical Reagent Co., Ltd.

Experimental

The experimental process for pretreatment of EMR and RM is shown in Fig. 1. EMR and RM were put into a 250-ml beaker according to a certain mass ratio. Then different proportions of deionised water were added and stirred for a certain time (as shown in Table 1). After stirring, the filter cake and first filtrate were obtained by filtration. The filter cake was dried (105 ℃) and ground to a particle size of < 200 mesh. A total of 10 g ground filter cake and 100 ml deionised water were added into a conical flask, and the resultant mixture was shaken at a shaking frequency of 110 ± 10 $r{\cdot}min^{-1}$ for 8 h, statically placed for 16 h and filtered to obtain the secondary filtrate.

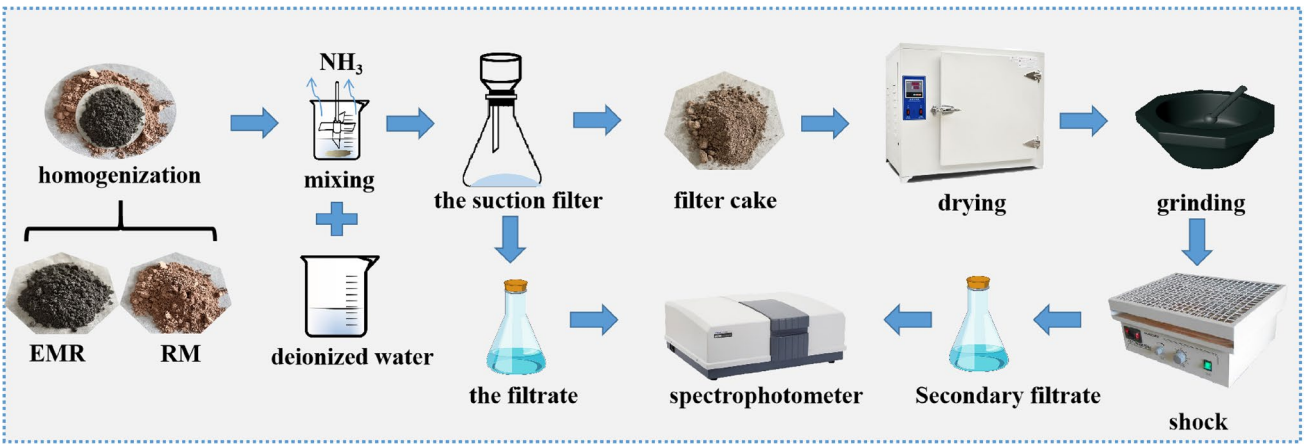

Fig. 1 Experimental flowchart of the collaborative stable curing of EMR and RM

Table 1 Experimental conditions of EMR and RM mutual processing experiment

Experiment	Mass ratio (EMR:RM)	Liquid–solid ratio	Mixing time (min)	Temperature	Revolution speed
A	1:1	1:1	0	25 ℃	300 r/min
			80		
			160		
			240		
			320		
B	5:1	1:1	320	25 ℃	300 r/min
	4:1				
	3:1				
	2:1				
	1:1				
C	1:1	0.6:1	320	25 ℃	300 r/min
		0.8:1			
		1:1			
		1.2:1			
		1.4:1			

The Mn^{2+} concentration was measured using the potassium periodate spectrophotometric method following the Chinese standard GB11906-89 (Deng et al. 2021). The NH_4^+–N concentration was measured using the nano-reagent spectrophotometric method, following the Chinese standard HJ535-2009. The average values of the results of six parallel measurements were considered the final test results. The ion concentration measured for the first filtrate was the soluble manganese ion concentration in the filtrate after the reaction, whereas that measured for the secondary filtrate was the soluble manganese ion concentration and the NH_4^+–N remaining in the filter cake after the reaction. The manganese-ion solidification ratio and the NH_4^+–N removal ratio were calculated using Eqs. (1) and (2):

$$S_{Mn^{2+}} = \frac{C^0{}_{Mn^{2+}} - C^1{}_{Mn^{2+}} - C^2{}_{Mn^{2+}}}{C^0{}_{Mn^{2+}}} \times 100\% \quad (1)$$

$$R_{NH_4^+-N} = \frac{C^0{}_{NH_4^+-N} - C^2{}_{NH_4^+-N}}{C^0{}_{NH_4^+-N}} \times 100\% \quad (2)$$

where *S*Mn2+ denotes the manganese-ion solidification ratio; *C*0Mn2+ denotes the total concentration of soluble manganese ions in EMR; *C*1Mn2+ and *C*2Mn2+ denote the concentrations of soluble manganese ions in the primary filtrate and secondary filtrate, respectively; $R_{NH_4^+-N}$ denotes the removal ratio of NH4+–N; $C^0{}_{NH_4^+-N}$ denotes the total concentration of NH4+–N in EMR and $C^2{}_{NH_4^+-N}$ denotes the concentration of NH4+–N in the secondary filtrate.

Characterisation

The chemical compositions of the original EMR and RM were determined using an X-ray fluorescence analyser under the following test conditions: an incident light energy of 16.4 keV, a spot size of 100 μm × 100 μm, an energy resolution of less than 2×10^{-4}, an information acquisition time of 3 min, parallel cross-section polished line scan, and an information acquisition time of 3 s per point of the line scan.

The mineral compositions of the original EMR, original RM, and treated EMR were determined via X-ray diffraction (XRD). The test strip was supplied with a tube voltage of 40 kV and a tube current of 30 mA; the continuous scanning range was 5–90°, the scanning speed was 2°/min, and the step width was 0.2°. The data were analysed using the MDI Jade 9 software.

The functional or EMR groups after treatment were identified via Fourier transform infrared (FTIR) spectroscopy. The test conditions were as follows: a wavelength range of 7800–350 cm^{-1}, a spectral resolution higher than 0.09 cm^{-1}, a sensitivity higher than 55,000:1, and a wavenumber accuracy of 0.01 cm^{-1}.

Scanning electron microscopy (SEM) and energy-dispersive spectrometry (EDS) were performed to observe the microscopic morphology of the EMR sample after treatment. The test conditions were as follows: an accelerating voltage of 0.1–30 kV, an electron beam current of 1 pA–2 nA, a sample chamber vacuum of 10^{-4} Pa, an effective area of the energy spectrum detector of 50 mm^2, and an energy resolution Mn Kα higher than 127 eV.

The valence or binding state changes of EMR elements after treatment were determined via X-ray photoelectron spectroscopy (XPS). The excitation source was a monochromatic Al Kα source, the power was 200 W, the spot size was 500 μm, the binding energy was corrected using the C(1 s) peak (284.8 eV) of alkyl carbon or contaminated carbon, and the essential vacuum during analysis was approximately 2×10^{-9} bar. Advantage analysis software was used to complete the data analysis and processing.

An electron probe microanalyser (EPMA) was used to determine the element correlation and distribution of EMR after treatment. The test conditions were as follows: a voltage of 20 kV, a current of 20 nA, and a beam spot diameter of 5 μm.

The heavy metal element content in the EMR leaching solution before and after treatment was measured via inductively coupled plasma (ICP) atomic emission spectroscopy (AES, ICP-AES). The test conditions were as follows: a spectral range of 7800–350 cm^{-1}, a resolution of 0.5 cm^{-1}, and a signal-to-noise ratio of 30,000:1 (P–P).

Results and discussion

Component analysis of EMR and RM

The chemical composition and phase composition of EMR and RM are shown in Table 2 and Fig. 2, respectively. Table 1 shows that the chemical composition of EMR is mainly SiO_2, CaO, Al_2O_3 and SO_3 (mass fraction 85.34%). Additionally, EMR also contains a small amount of Fe_2O_3, MnO, MgO, K_2O, etc. The mass fraction of the harmful heavy metal MnO is 3.33%. The chemical composition of RM is mainly SiO_2, CaO, Al_2O_3, and Fe_2O_3 (mass fraction of 83.86%). Additionally, RM also contains a small amount of Na_2O, K_2O, MgO, etc. Na_2O and K_2O mainly exist in a strong alkaline form, and their mass fraction is 8.12%. Figure 2 shows that the phase composition of EMR is mainly $CaSO_4{\cdot}2H_2O$, SiO_2, $KAl_2AlSi_3O_{10}(OH)_2$, $CaAl_2Si_2O_8{\cdot}4H_2O$, $(NH_4)_2(Mn,Fe,Mg)(SO_4)_2{\cdot}6H_2O$, and $(NH_4)_2SO_4$. $(NH_4)_2(Mn,Fe,Mg)(SO_4)_2{\cdot}6H_2O$ and $(NH_4)_2SO_4$ are the main forms of manganese and ammonia nitrogen in EMR (Yang et al. 2014; Shu et al. 2018). The phase composition of RM is mainly Fe_2O_3, $CaCO_3$, Al_2O_3, $Na_2O{\cdot}Al_2O_3{\cdot}6SiO_2$, $Na_4(Al_2Si_3O_{12})Cl$, $(Na,K,Ca)_{3-4}[(Si,Al_6)O_{12}][SO_4,CO_3,Cl]{\cdot}nH_2O$, $Ca_2Al_2(SiO_4)(OH)_8$, and AlOOH. $Na_2O{\cdot}Al_2O_3{\cdot}6SiO_2$, $Na_4(Al_2Si_3O_{12})Cl$, $(Na,K,Ca)_{3-4}[(Si,Al_6)O_{12}][SO_4,CO_3,Cl]{\cdot}nH_2O$, Ca_2Al_2 $(SiO_4)(OH)_8$, and AlOOH are some existing forms of alkaline substances in RM (Luo et al. 2017). It is worth noting that previous studies have shown that some alkaline substances in RM still exist in the form of amorphous sodium oxide, potassium oxide, and magnesium oxide (Li et al. 2020; Liu et al. 2017).

Influence of treatment conditions on treatment effect

Effect on ammonia nitrogen removal ratio and manganese ion solidification ratio

Figure 3 illustrates the effect of treatment conditions on the ammonia–nitrogen removal ratio and manganese-ion solidification ratio. Figure 3 a shows that when the stirring time was increased from 0 to 240 min, the ammonia nitrogen removal ratio increased from 79.22 to 85.36%, a remarkable increase of 6.14%. This is because a prolonged stirring time

Table 2 Chemical composition of EMR and RM (wt.%)

	SiO_2	CaO	Al_2O_3	SO_3	Fe_2O_3	MnO	Na_2O	K_2O	MgO	TiO_2	Other
EMR	25.17	16.99	7.30	35.88	3.81	3.33	0.53	1.74	3.28	0.38	1.59
RM	21.77	16.40	27.63	1.04	18.06	0.04	6.14	1.98	1.29	4.87	0.78

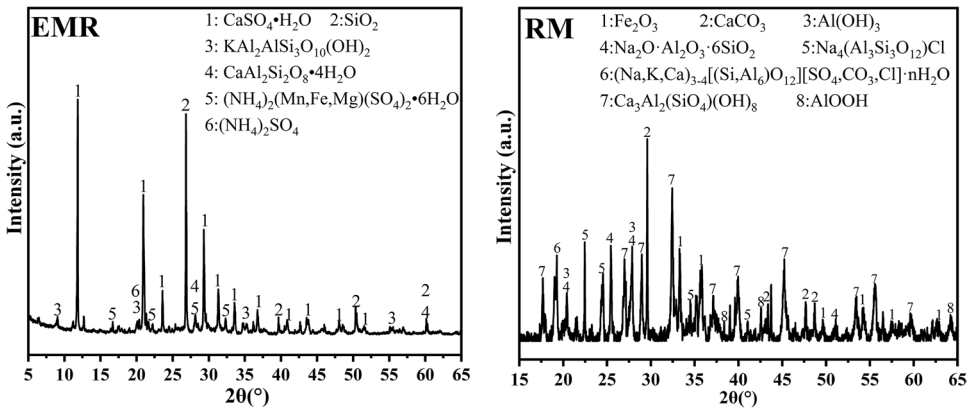

Fig. 2 XRD patterns of EMR and RM

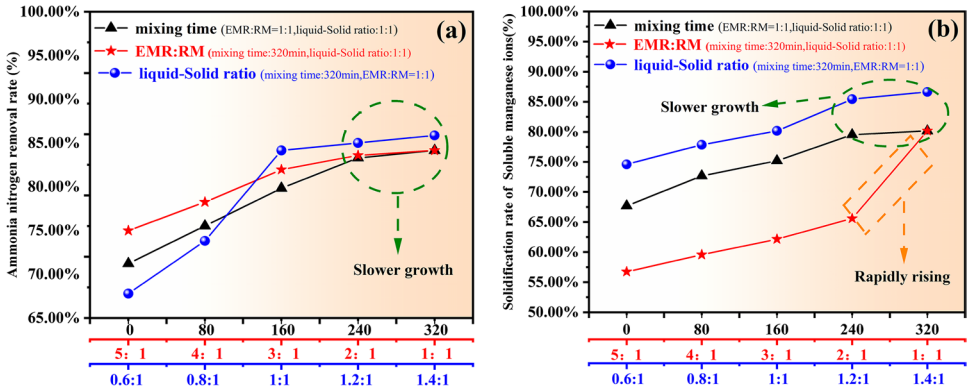

Fig. 3 Effects of treatment conditions on ammonia nitrogen removal ratio and manganese ion solidification ratio

favours the continuous reaction between the alkaline substance and ammonia nitrogen. The removal ratio of ammonia nitrogen increased from 83.29 to 84.15% when the stirring time was extended to 320 min. The increase in the removal ratio of ammonia was < 1%, which can be attributed to the gradual depletion of ammonia nitrogen during the reaction of ammonia nitrogen with alkaline substances, making the ammonia removal reaction approach the endpoint. When the EMR:RM mass ratio was increased from 5:1 to 2:1, the ammonia nitrogen removal ratio increased from 74.98 to 83.59%. This substantial increase can be attributed to the increase in the concentration of alkaline substances in the system owing to the increase in the RM content, which promotes the progress of the ammonia removal reaction. When the EMR:RM mass ratio was increased from 2:1 to 1:1, the ammonia nitrogen removal ratio increased from 83.59 to 84.15%. The increase in removal ratio was < 0.6%. This was because the concentration of the alkaline substances in the system was approximately equal to the concentration required for the complete removal of ammonia nitrogen (the part that can be removed). When the liquid–solid ratio increased from 0.6:1 to 1.2:1, the ammonia nitrogen removal ratio increased from 67.78 to 85.01%, a substantial increase of 17.23%. This remarkable increase was attributed to the increased liquid content, which made it easier for the alkaline substances in RM to dissolve and react with ammonia nitrogen in EMR (Zhang et al. 2012). When the liquid–solid ratio was increased from 1.2:1 to 1.4:1, the ammonia nitrogen removal ratios increased from 85.01 to 85.87%. The increase in the removal ratio was < 0.9%. This was because the alkaline substances were almost completely dissolved, and increasing the liquid content no longer assisted in increasing the concentration of alkaline substances in the system.

Figure 3 b shows that when the stirring time was prolonged from 0 to 240 min, the manganese-ion solidification ratio increased from 67.69 to 79.53%. This is because the prolongation of stirring time is also beneficial to the continuous reaction of alkaline substances in RM with soluble manganese ions in EMR. When the stirring time exceeded 240 min and was above 320 min, the ratio of manganese-ion solidification increased from 79.53 to 80.16%. The increase is less than 0.7%. This is because the solidification reaction of manganese ions is also near the endpoint within 320 min. When the EMR:RM mass ratio was increased from 5:1 to 2:1, the manganese-ion solidification ratio increased from 56.75 to 65.59%. This gradual increase can be attributed to the fact that the ammonia removal reaction in the system preferentially consumes majority of alkaline substances. Therefore, fewer alkaline substances remain for the solidification reaction of manganese ions. When the EMR:RM mass ratio was increased from 2:1 to 1:1, the manganese-ion solidification ratio increased from 65.59 to 80.16%. This substantial increase occurred because the ammonia removal reaction in the system approached the endpoint and the subsequent dissolved alkaline substances were utilised mainly in the manganese solidification reaction. When the liquid–solid ratio was increased from 0.6:1 to 1.2:1, the manganese-ion solidification ratio increased from 74.59 to 85.44%. This was because the increase in liquid content promoted the dissolution of alkaline substances, which was also beneficial to the manganese-ion solidification reaction. When the liquid–solid ratio was increased from 1.2:1 to 1.4:1, the manganese-ion solidification ratio increased from 85.44 to 86.63%. The increase is less than 1.2%. This was because the alkaline substances were completely dissolved, and increasing the liquid content no longer assisted in increasing the alkaline content in the system, thus not promoting the manganese-ion solidification reaction.

The change of phase composition in the system

The FTIR and XRD patterns of samples treated under different conditions are shown in Figs. 4 and 5, respectively. When the stirring time was increased from 0 to 240 min, the intensities of the N–H–N absorption peaks considerably decreased (Chen et al. 2022), the Mn–OH and Mn–O absorption peaks considerably increased (Fig. 4 a) (Peng et al. 2010; Shu

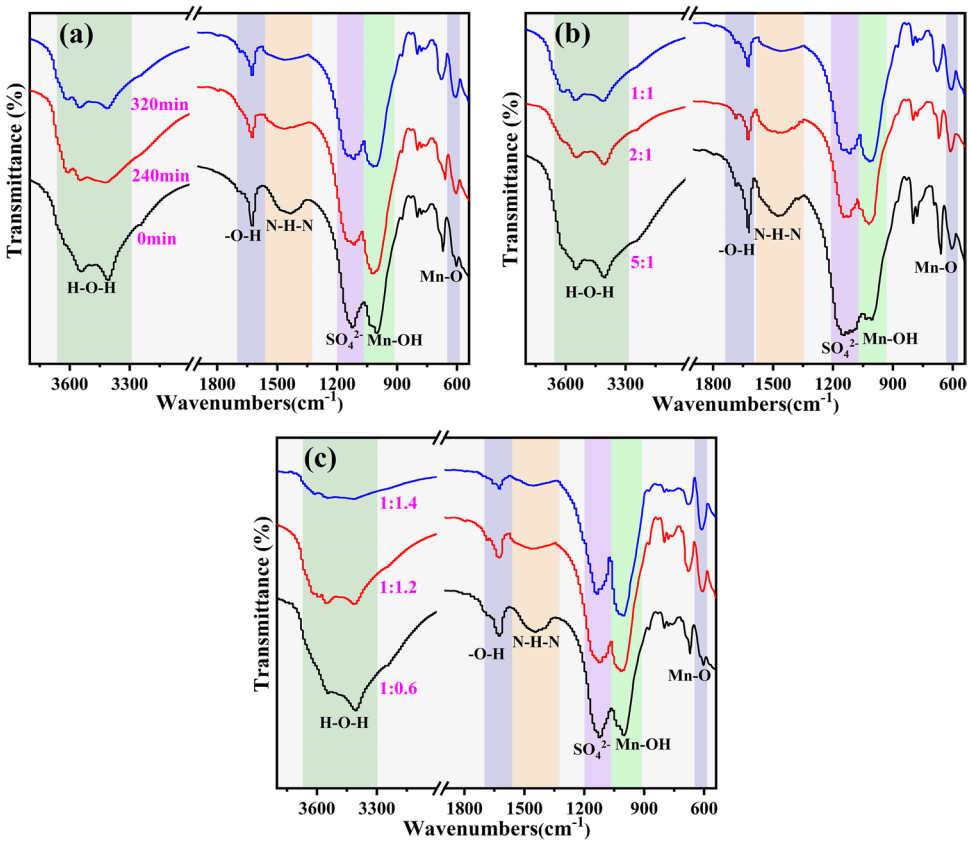

Fig. 4 FTIR spectra with different reaction conditions **a** mixing time; **b** EMR–RM; **c** solid–liquid ratio

et al. 2021). The intensities of the $(NH_4)_2$ $Mg(SO_4)_2$ and $(NH_4)_2SO_4$ peaks considerably decreased, the KMn_8O_{16} and $Mn_{3.88}O_7(OH)$ peaks considerably increased (Fig. 5 a). This was because, with the prolongation of stirring time, ammonia nitrogen, soluble manganese ions, and alkaline substances continued to react according to the pathways shown in Eqs. (1)–(4) (Table 3). When the stirring time was extended to 320 min, the intensities of the absorption N–H–N and Mn–OH absorption peaks slightly decreased, and the absorption peak of Mn–O was enhanced (Fig. 4 a). The peak of $(NH_4)_2$ $Mg(SO_4)_2$ almost disappeared, the peaks of $(NH_4)_2SO_4$ and $Mn_{3.88}O_7(OH)$ slightly weakened, and the peak of KMn_8O_{16} slightly increased (Fig. 5 a). This indicates that when the stirring time reached 320 min, the ability of RM to treat ammonia nitrogen and manganese ions reached the limit. The hydroxylation reaction precedes the oxidation reaction in the solidifying process of manganese ions. Notably, the intensity of the $Mg_3O(CO_3)_2$ peak considerably increased with increasing stirring time (Fig. 5 a). This can be attributed to the gradual reaction of $Mg(OH)_2$ and CO_2 to form $Mg_3O(CO_3)_2$ (Eq. (5) in Table 3). Concurrently, the intensities of the Na_2SO_4 and $CaCO_3$ peaks considerably increased, whereas that of the $CaSO_4{\cdot}2H_2O$ peak gradually decreased (Fig. 5 a). This was because the amorphous Na_2O reacted with water to form NaOH, and partial NaOH reacted with the $CaSO_4{\cdot}2H_2O$ crystal phase to form $Ca(OH)_2$ and Na_2SO_4 (Eqs. (6) and (7) in Table 3). $Ca(OH)_2$ further reacted with the carbonate to form $CaCO_3$ (Eqs. (8) in Table 3). The reaction of NaOH with $CaSO_4{\cdot}2H_2O$ etched and broke the $CaSO_4{\cdot}2H_2O$ crystal, allowing alkaline substances to enter the $CaSO_4{\cdot}2H_2O$ crystal and react with eutectic ammonia nitrogen. This was considerably beneficial for the removal of ammonia nitrogen. When the RM content was increased from 5:1 to 2:1, the intensity of the N–H–N absorption peak considerably decreased, and the Mn–OH and Mn–O absorption peaks considerably increased (Fig. 4 b). The intensities of the $(NH_4)_2$ $Mg(SO_4)_2$ and $(NH_4)_2SO_4$ peaks considerably decreased, the $Mn_{3.88}O_7(OH)$ and KMn_8O_{16} peaks considerably increased (Fig. 5 b). When the RM content was increased from 2:1 to 1:1, the intensity of the N–H–N absorption peak continued to weaken, and the absorption peaks of Mn-OH and Mn–O continued to increase (Fig. 4 b). The intensity of the $(NH_4)_2SO_4$ peak continuously decreased, the peak of $(NH_4)_2$ $Mg(SO_4)_2$ is basically unchanged. The intensities of the $Mn_{3.88}O_7(OH)$ and KMn_8O_{16} peaks continuously increased. This observation is consistent with the experimental results presented in Fig. 3. The increase in the RM content also increased the concentration of alkaline substances in the system, thus promoting the removal of ammonia and solidification of manganese ions. Additionally, with an increase in the RM content, the intensity of the $CaSO_4{\cdot}2H_2O$ peak gradually

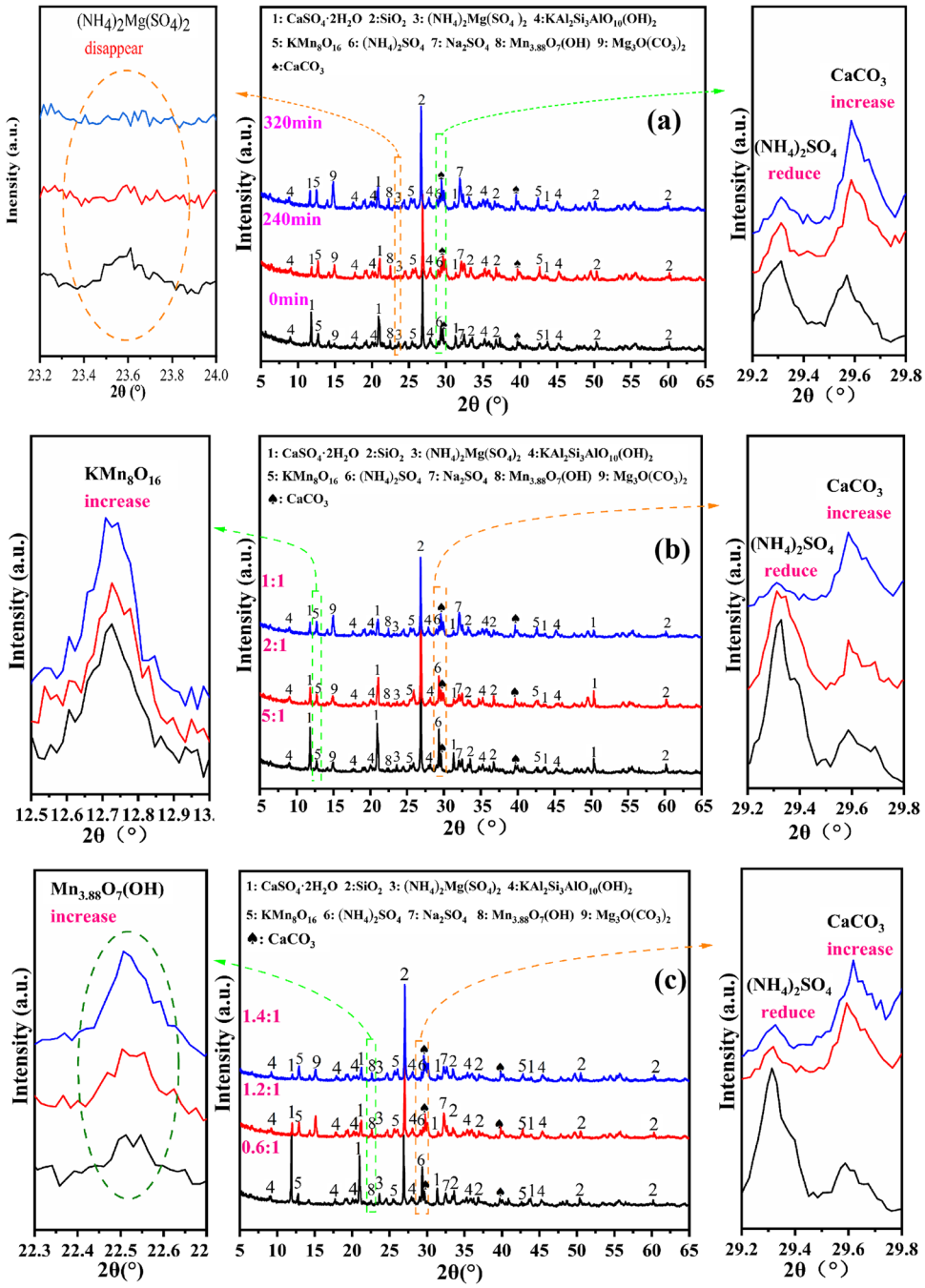

Fig. 5 XRD patterns of samples under different treatment conditions (**a** EMR:RM = 1:1, liquid–solid ratio = 1:1; **b** mixing time = 320 min, liquid–solid ratio = 1:1; **c** EMR:RM = 1:1, mixing time = 320 min)

decreased, whereas those of the Na_2SO_4 and $CaCO_3$ peaks gradually increased. This result indicates that the increased concentration of alkaline substances will also promote the process of etching and destroying $CaSO_4{\cdot}2H_2O$ crystals and eliminating eutectic ammonia nitrogen.

When the liquid–solid ratio increased from 0.6:1 to 1.2:1, and the intensity of the N–H–N absorption peak considerably decreased, the Mn–OH and Mn–O absorption peaks considerably increased (Fig. 4 c). The intensities of the $(NH_4)_2\,Mg(SO_4)_2$, $(NH_4)_2SO_4$ and $CaSO_4{\cdot}2H_2O$ peaks considerably decreased, the $CaCO_3$, Na_2SO_4, $Mn_{3.88}O_7(OH)$, and KMn_8O_{16} peaks considerably increased (Fig. 5 c). This was because the increase in the liquid content caused more alkaline substances to dissolve out and participate in the reactions of ammonia removal, manganese solidification, and the etching of $CaSO_4{\cdot}2H_2O$. When the liquid–solid ratio continued to increase to 1.4:1, the intensity of the N–H–N absorption peak slightly decreased, and the absorption peaks of Mn–OH and Mn–O are slightly enhanced (Fig. 4 c). The $(NH_4)_2\,Mg(SO_4)_2$, $(NH_4)_2SO_4$, $Mn_{3.88}O_7(OH)$, KMn_8O_{16}, $CaSO_4{\cdot}2H_2O$, and $CaCO_3$ peaks did not exhibit any distinct change; however, the intensity of the Na_2SO_4 peak

Table 3 Reaction equations in the mutual treatment system of EMR and RM

Equation	Number
$NH_4^+(aq) + OH^-(aq) \rightarrow NH_3(g) + H_2O$	(1)
$8Mn^{2+}(aq) + 16O_2\ (g) + K^+(aq) \rightarrow KMn_8O_{16}(s)$	(2)
$MnSO_4(s) + 2OH^-(aq) \rightarrow Mn(OH)_2(aq) + SO_4^{2-}(aq)$	(3)
$3.88Mn(OH)_2(aq) + 1.56O_2(g) \rightarrow Mn_{3.88}O_7(OH)(s) + 3.88H_2O$	(4)
$3\ Mg(OH)_2(aq) + 2CO_2\ (g) \rightarrow Mg_3O(CO_3)_2(s) + 3H_2O$	(5)
$Na_2O + H_2O = 2NaOH$	(6)
$2NaOH + CaSO_4{\cdot}2H_2O = Na_2SO_4 + Ca(OH)_2 + 2H_2O$	(7)
$Ca^{2+}(aq) + CO_3^{2-}(aq) \rightarrow CaCO_3(s)$	(8)

considerably decreased (Fig. 5 c). This was because all the alkaline substances were dissolved, and the increase in the liquid content did not help in increasing the content of alkaline substances in the system. In other words, the increase in liquid content is not conducive to the promotion of ammonia removal, manganese solidification, and the etching of $CaSO_4{\cdot}2H_2O$. Furthermore, the increased liquid content made the solution unsaturated, dissolving part of Na_2SO_4; therefore, the intensity of the Na_2SO_4 peak decreased.

The XPS spectra of EMR obtained before and after the reaction under suitable conditions are shown in Fig. 6. The full XPS spectrum (Fig. 6 a) showed that when EMR reacted with RM, the characteristic peak of Mn was slightly increased (0.11% → 0.18%) and the characteristic peak of N was considerably weakened (18.93% → 4.74%). These findings were attributed to the reaction of the alkaline substances in RM with ammonia and manganese ions, respectively, which resulted in ammonia nitrogen removal and manganese-ion solidification. The Mn2p (Fig. 6 b) peak showed three characteristic peaks of Mn in the sample before the reaction. These characteristic peaks are the peaks of divalent Mn at 640.5 eV, trivalent Mn at 641.8 eV, and heptavalent Mn at 646.3 eV (Shu et al. 2019, Umezawa and Reilley 1978). A substantial amount of manganese in EMR is in the form of divalent manganese, with trace amounts in the form of trivalent and heptavalent manganese. Divalent manganese is produced via acid leaching of manganese ore and remains in EMR. The trivalent and heptavalent manganese may be present owing to oxidation of manganese ions as a result of long-term open storage of EMR. After the reaction with RM, there is a considerable weakening of the divalent manganese peak and the disappearance of the trivalent manganese peak. At the same time, a new characteristic peak appears near the binding energy of 642.6 eV. Trivalent manganese corresponds to a binding energy usually around 641.8 eV, whereas tetravalent manganese corresponds to a binding energy usually around 643.4 eV (Dong et al. 2002). As 642.6 eV is between 641.8 and 643.4 eV, the valence of the manganese ions after this reaction is between

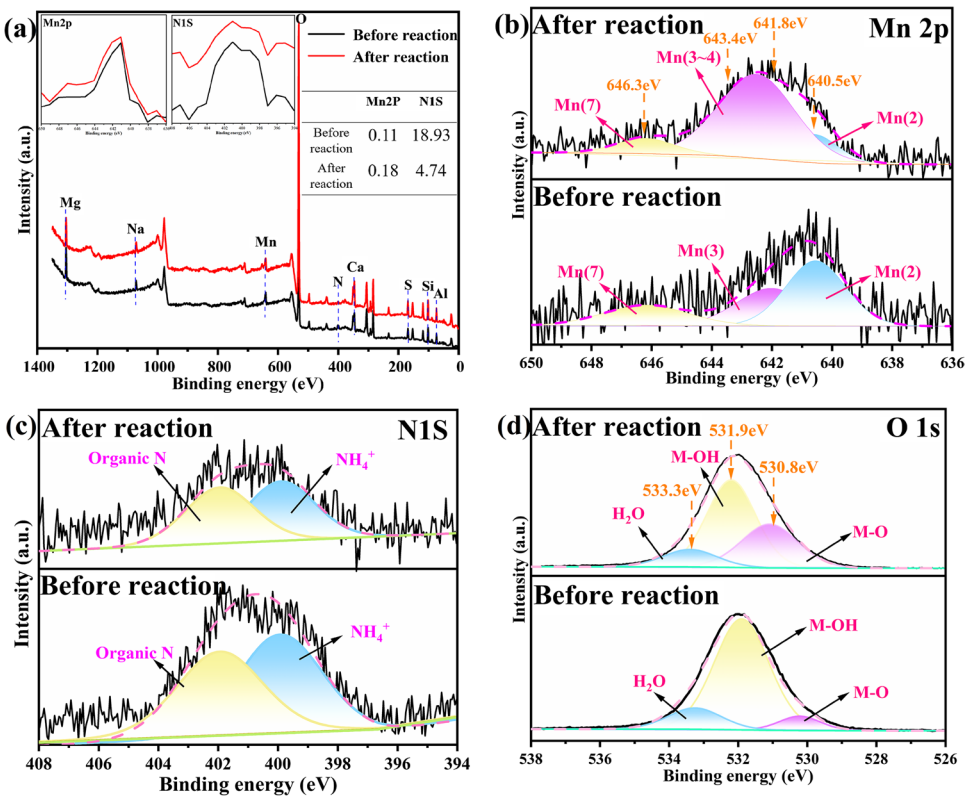

Fig. 6 XPS spectra of EMR before and after reaction under suitable conditions (**a** XPS full spectrum; **b** Mn 2p XPS spectra; **c** N1S XPS spectra; **d** O 1S XPS spectra)

trivalent and tetravalent. This is because a large amount of divalent and trivalent manganese in EMR reacts with RM and is converted to manganese, which is between trivalent and tetravalent. The N1s (Fig. 6 c) peak shows that nitrogen before and after the reaction had two characteristic peaks: the peak corresponding to the ammonium ion near 400 eV (Umezawa and Reilley 1978) and that to organic nitrogen near 402 eV (Li et al. 2020; Distefano et al. 1976). After the reaction of EMR with RM, the peaks corresponding to the ammonium ion and organic nitrogen were considerably weakened. Because the alkaline substance reacts with the ammonium ion, the ammonium ion is converted into ammonia gas and discharged, thereby weakening the peak of the ammonium ion. In an aqueous solution, part of the organic nitrogen is dissolved, weakening the peak of organic nitrogen. The O1s peak of the EMR before the reaction (Fig. 6 d) can be divided into three peaks: M–O (530.8 eV), M–OH (531.9 eV), and a water molecule (533.3 eV) (Li et al. 2021, 2017; Mishra et al. 2021). After the reaction, the peaks of adsorbed water molecules exhibited no distinct change. The peak of M–OH considerably weakened, whereas that of M–O considerably increased. This shows that manganese ions react with alkaline substances and exist in the form of metal oxides. The change rule of the peaks of Mn2p, N1s, and O1s is another evidence of the effectiveness of the mutual harmless treatment of EMR and RM.

Process and mechanism analysis

Figure 7 depicts a schematic representation of the reaction process for the mutual harmless treatment of EMR and RM. The mutual harmless treatment of EMR and RM in an aqueous solution comprises two stages: stage I involves the rapid consumption of ammonia nitrogen, manganese ions, and alkaline substances. At this time, the ammonia removal rate and manganese fixation rate increased rapidly. In stage I, in an aqueous solution, $(NH_4)_2Mg(SO_4)_2$, $(NH_4)_2Mn(SO_4)_2$, and $(NH_4)_2SO_4$ in EMR dissolved out NH_4^+ and Mn^{2+}, the soluble alkali (NaOH, KOH, and Na_2CO_3) in RM was the first to dissociate OH^-. After NH_4^+ reacts with OH^-, NH_4^+ is converted to ammonia gas that is emitted (Wang et al. 2013; He et al. 2021a). After the Mn^{2+} reacts with OH^-, it is first converted into manganese hydroxide or manganese oxyhydroxide (Zhang et al. 2020). Subsequently, manganese hydroxide or manganese oxyhydroxide is oxidised and solidified as an oxide (such as KMn_8O_{16}) (Deng et al. 2021).

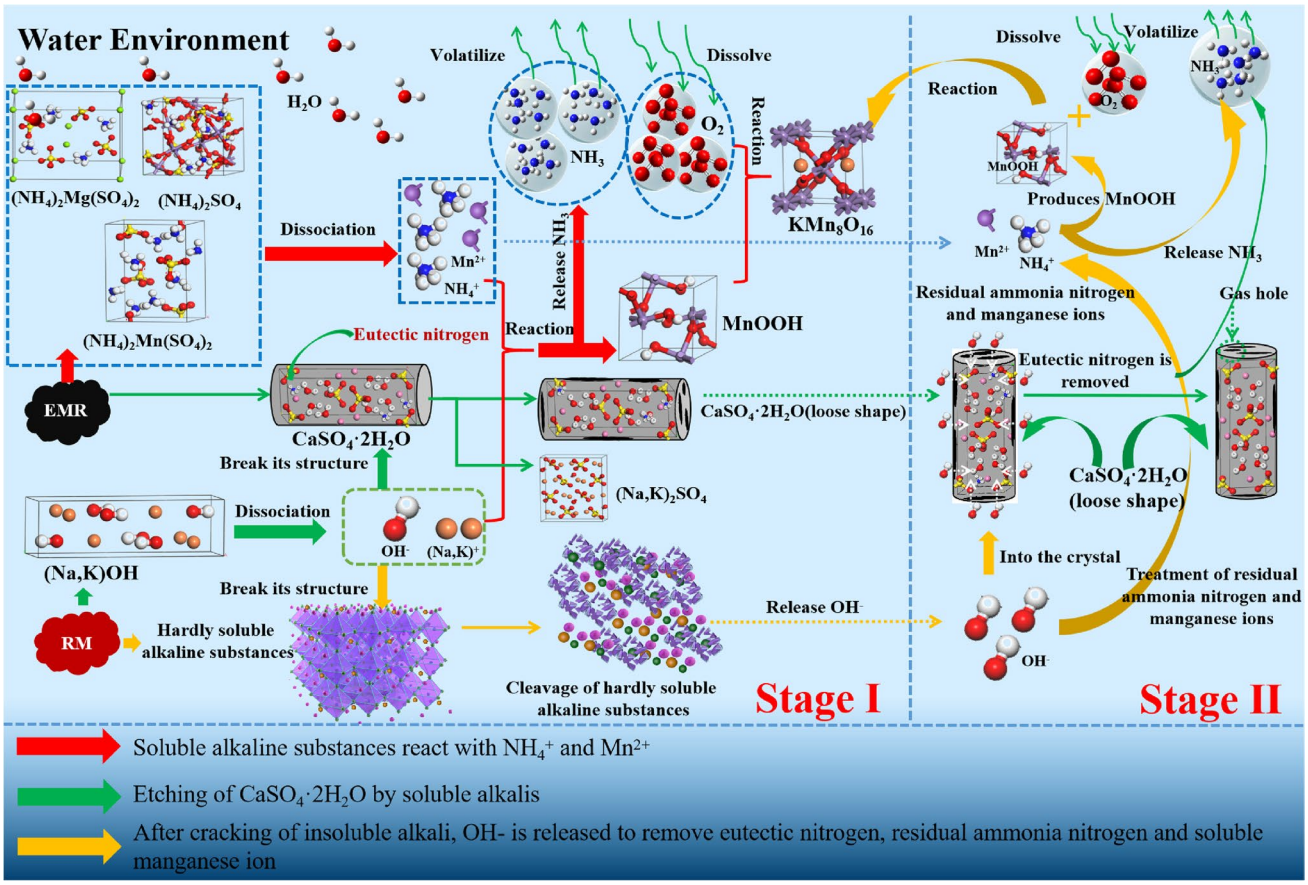

Fig. 7 Schematic diagram of the reaction mechanism of the mutually harmless treatment of EMR and RM

Simultaneously, the OH^- dissociated from the soluble alkali also reacted with $CaSO_4{\cdot}2H_2O$ and insoluble alkali for etching. This reaction destroyed the $CaSO_4{\cdot}2H_2O$ and insoluble alkali structures ($Na_2O{\cdot}Al_2O_3{\cdot}6SiO_2$, $Na_4(Al_3Si_3O_{12})Cl$, $Ca_3Al_2(SiO_4)(OH)_8$ and $(Na,K,Ca)_{3-4}[(Si,Al_6)O_{12})][SO_4,CO_3,Cl]\ nH_2O$), rendering their structures loose (Wang et al. 2018b; Liao et al. 2022; Liu et al. 2006). In stage II, residual ammonia nitrogen, manganese ions, and insoluble alkali in the system slowly consume each other. At this time, the ammonia removal ratio and the manganese solidification ratio increased very slowly and nearly stabilised. In stage II, the structures of the insoluble alkaline substances are destroyed and OH^- is gradually dissociated. These OH^- continue to react with the residual NH_4^+ and Mn^{2+} in the solution, resulting in NH_4^+ continuously transforming into ammonia gas that can escape and Mn^{2+} continuously converting into an oxide form and solidifying. Additionally, these OH^- penetrate the $CaSO_4{\cdot}2H_2O$ crystal and interact with the eutectic nitrogen, converting it into ammonia gas that can escape.

Process kinetic analysis

In this study, the ammonia nitrogen removal and the soluble manganese-ion solidification in EMR belonged to the solid–liquid reactions. For these reactions, a shrinkage modelling method is a good approach for investigating the kinetic reaction mechanism (Lan et al. 2021; Liu et al. 2022). Therefore, in order to clarify the kinetic mechanism of ammonia nitrogen removal and manganese solidification process in this study. The shrinkage model method is used for dynamic calculation and analysis. The main control mechanisms of the shrinkage model method were the membrane diffusion control mechanism, chemical reaction control mechanism, and the chemical reaction and membrane diffusion co-control mechanism.

The reaction equation was expressed as Eq. (9) when the chemical reaction controlled the reaction rate.

$$1-(1-x)^{(1/3)}=k_1t \tag{9}$$

The reaction equation was expressed as Eq. (10), when the reaction rate is controlled by membrane diffusion.

$$1-2x/3-(1-x)^{(2/3)}=k_2t \tag{10}$$

Meanwhile, the reaction equation was expressed as Eq. (11) when membrane diffusion and chemical reaction controlled the reaction rate.

$$\ln(1-x)/3+(1-x)^{(-1/3)}-1=k_3t \tag{11}$$

Figure 8 shows the kinetic fitting diagram of the ammonia nitrogen removal ratio and manganese-ion solidification ratio obtained through the shrinkage model method. Figure 8 a,b shows that the slopes of the fitted lines for the ammonia nitrogen removal and manganese-ion solidification ratios were greater than 0, indicating that the ammonia nitrogen removal ratio and manganese-ion solidification ratio gradually increased with reaction time. The ammonia nitrogen removal ratio and the manganese-ion solidification ratio showed the best fit with $\ln(1-x)/3+(1-x)^{(-1/3)}-1=k_3t$, depicting fitted variances of $R^2=0.9897$ and $R^2=0.9888$, respectively. Accordingly, $\ln(1-x)/3+(1-x)^{(-1/3)}-1=k_3t$ corresponded to the co-control mechanism of membrane diffusion and chemical reactions. In the process of mutual treatment of EMR and RM, the dissolution of the ammonia nitrogen, soluble manganese ions, and alkaline substances first occurred. During this time, solid-phase molecules cleaved into the ions and diffused across the liquid-phase (water) boundary film into the liquid-phase body. Therefore, the dissolution process of ammonia nitrogen, soluble manganese ions, and alkaline substances was controlled by the membrane diffusion mechanism. After ammonia nitrogen,

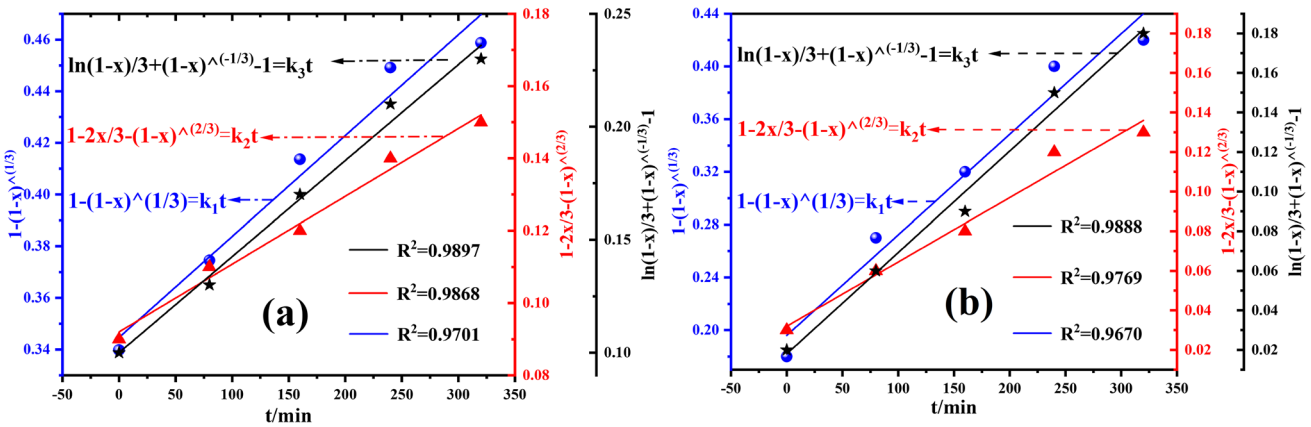

Fig. 8 Kinetic model fitting line for ammonia nitrogen and manganese leaching. (**a**, **b** EMR:RM = 1:1, solid–liquid ratio = 1:1.4)

soluble manganese ions and alkaline substances were dissolved into the liquid phase, the ammonia nitrogen, manganese and OH^- ions combined to react and produce ammonia and solidified manganese precipitation. In this process, the control mechanism was mainly the chemical reaction control mechanism. Thus, the whole EMR–RM interaction process was controlled by the membrane diffusion and chemical reaction mechanisms.

Elemental distribution and microstructure of the treated samples

Elemental distribution analysis

The EPMA surface scan mapping of the treated samples under suitable conditions is presented in Fig. 9, and the correlation scatter plots of the samples treated under suitable conditions are presented in Fig. 10. Figure 9 indicates that in the area where Mn elements were relatively concentrated, O and K were also slightly concentrated (the area shown by the red square). Meanwhile, the scatter plots of Mn–K, Mn–O, and K–O (shown in Fig. 10) show that when the contents of K and O were less than 0.5 wt%, 6.2 wt%, and 7.9 wt%, respectively, the contents of Mn–K, Mn–O, and K–O showed a distinct positive correlation. Manganese was predominantly solidified in the samples as $Mn_{3.88}O_7(OH)$ and KMn_8O_{16}, demonstrating minor quantities of Mn–O and K–O compounds in the sample following the reaction. In the area where Al elements were comparatively concentrated, Na was relatively concentrated (the area shown by the red circle in Fig. 9). Meanwhile, it can be observed in scatter plots that when the content of Al was lower than 2.0 wt%, the content of Na–Al showed a distinct positive correlation. This indicates that many Na–Al compounds remained in the pretreated samples, owing to large amount of albite formed with incorporation of RM. Na and O elements were likewise considerably concentrated in places where S elements were concentrated (the area shown by the red hexagon in Fig. 9). Moreover, the scatter plots of Na–O and S–Na show that when the contents of O and Na were lower than 14 and 1.5 wt%, respectively, the contents of Na–O and S–Na showed a positive correlation. This indicates that Na_2SO_4 existed in the sample after the

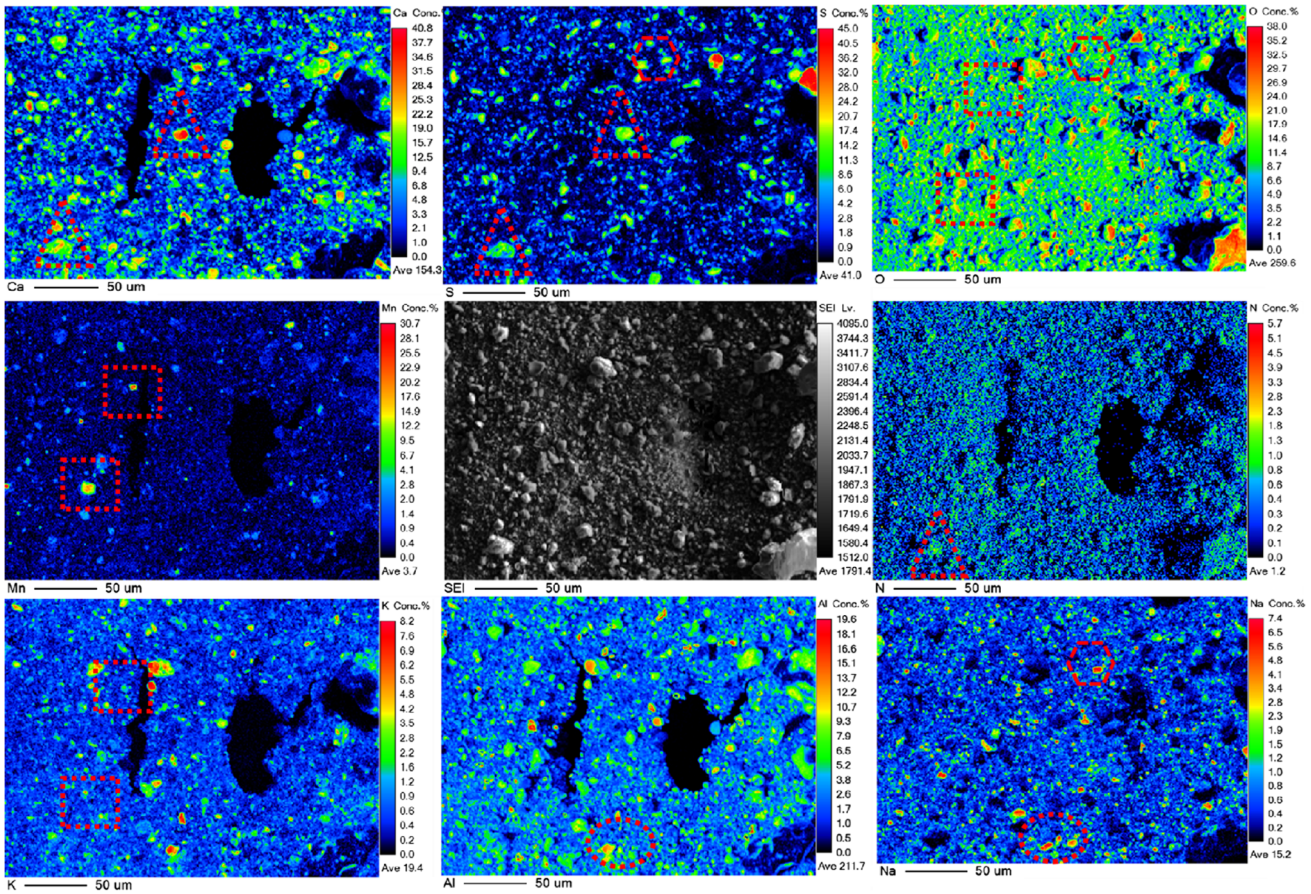

Fig. 9 Electron probe microanalyser (EPMA) surface scan mapping of treated samples under suitable conditions

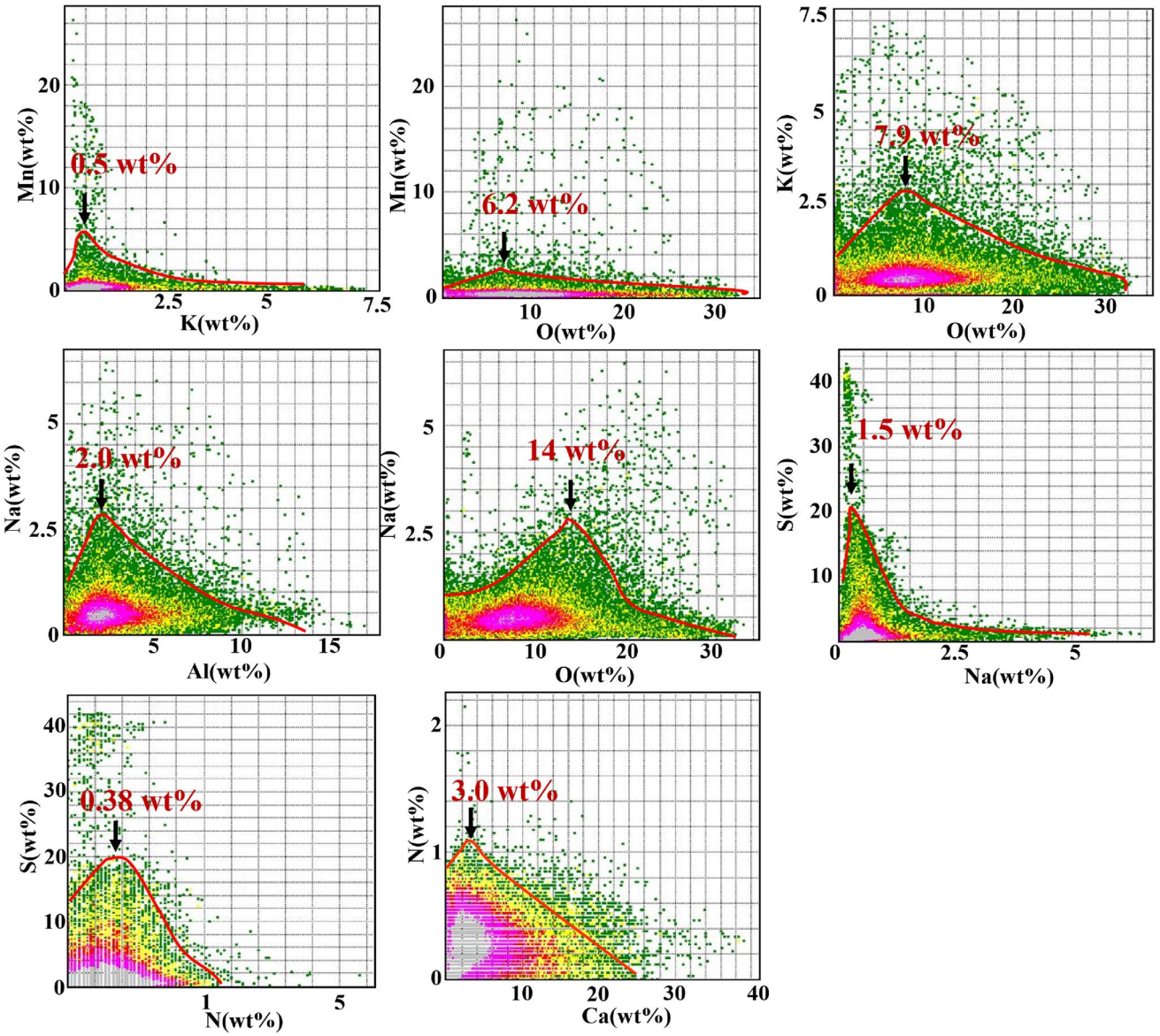

Fig. 10 Element correlation scatter plots of sample after preprocessing

reaction. Notably, in the area where Ca and S elements were relatively concentrated ($CaSO_4 \cdot 2H_2O$), N elements were also relatively concentrated (the area shown by the red triangle in Fig. 9). Furthermore, the N–S and N–Ca scatter plots show that when the N and Ca contents were lower than 0.38 and 3.0 wt%, respectively, the contents of N–S and N–Ca showed a distinct positive correlation. This indicates that a small amount of ammonia nitrogen is likely to exist in EMR in a eutectic form along with $CaSO_4 \cdot 2H_2O$. The etching reaction of alkaline substances and $CaSO_4 \cdot 2H_2O$ is an effective means to remove eutectic nitrogen.

Microstructure analysis

The SEM morphologies of the samples treated under suitable conditions are shown in Fig. 11. Figure 11 a shows that bulk $CaSO_4 \cdot 2H_2O$ with loose structures and pores appeared in the sample. This morphology of $CaSO_4 \cdot 2H_2O$ can be caused by the following two reactions: first, the etching reaction of alkaline substances to $CaSO_4 \cdot 2H_2O$, and second, the reaction of alkaline substance with the eutectic ammonia nitrogen, converting the eutectic ammonia nitrogen into ammonia gas, which escapes and leaves pores on the surfaces. Figure 11 b and the corresponding

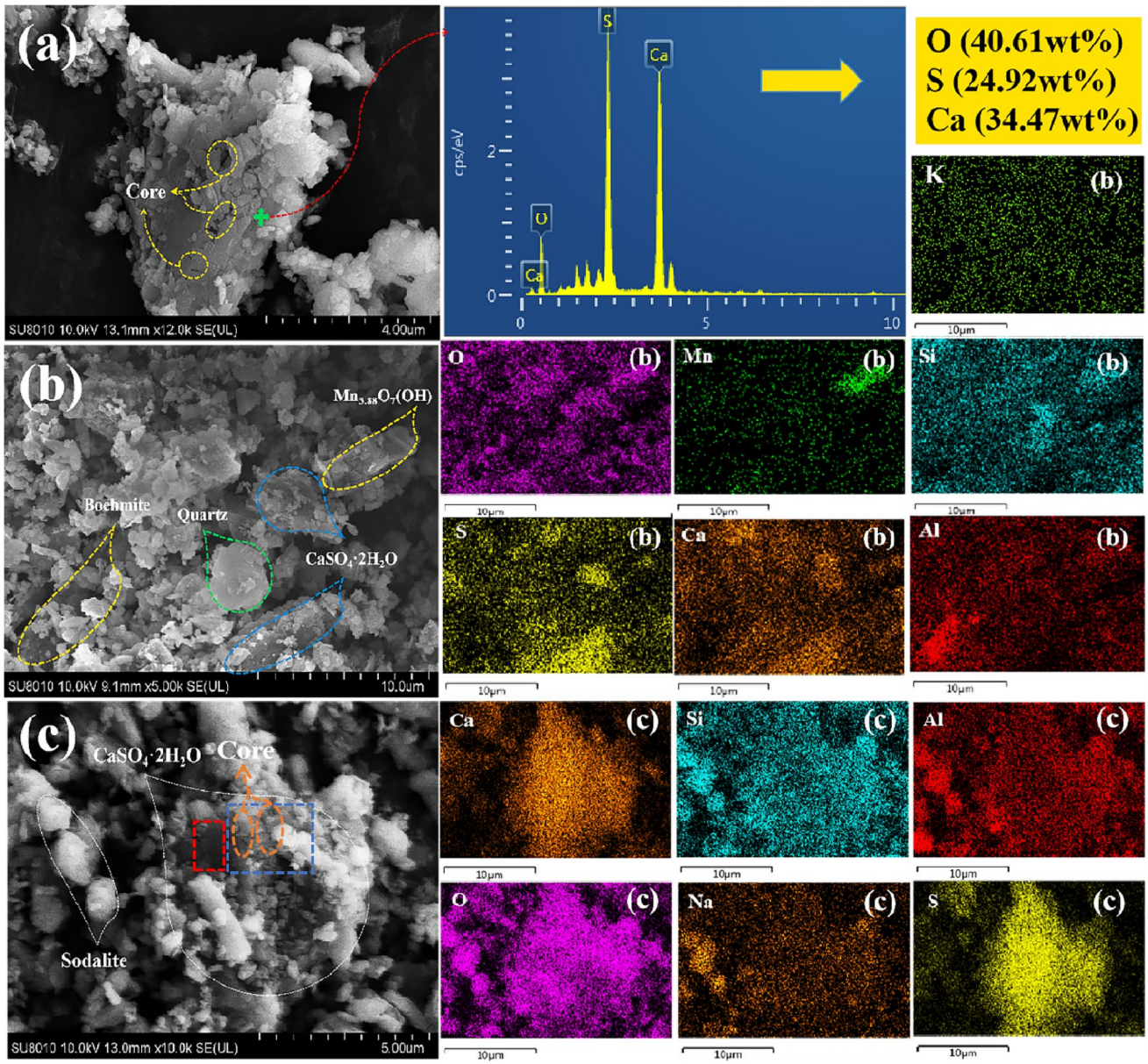

Fig. 11 Micromorphology of treated samples under suitable conditions

EDS scan results show that in the treated samples, $Mn_{3.88}O_7(OH)$ mainly existed in the form of bar-like aggregates, and KMn_8O_{16} was mainly distributed in the sample as fine debris. Furthermore, quartz and residual boehmite (AlOOH) were formed in smooth slab-like and rod-like shapes, respectively. Figure 11 c and the corresponding EDS scan results show that in the treated sample, the residual sodalite existed as small lumps. Notably, the surface of some bulk $CaSO_4{\cdot}2H_2O$ exhibited both a relatively flat region (red line box) and relatively loose region (blue line box). No pores were found in the relatively flat areas; however, pores could be found in looser areas. This shows that the etching reaction of $CaSO_4{\cdot}2H_2O$ by the

Table 4 Heavy metal leaching concentrations of EMR, RM, and ER

Sample	Content ($mg{\cdot}L^{-1}$)				
	Cr	Cu	Mn	Ni	Zn
EMR	116	42.9	1460	81.8	147
RM	246	402	/	92.2	80.34
ER	1.45	0.099	198	0.294	0.449

alkaline substances is beneficial for removing eutectic ammonia nitrogen.

Effect of the treatment process on the leaching concentration of heavy metals

Table 4 presents the heavy metal leaching concentrations of the EMR, RM, and mutually treated (under suitable conditions) samples (ER). As shown in the table, the manganese ion leaching concentration in EMR before the mutual treatment was 1460 mg·L^{-1}, whereas that of ER after the mutual treatment was 198 mg·L^{-1}. The manganese ion leaching concentration considerably decreased because the soluble manganese ions in EMR were well solidified after the mutual treatment. Before the mutual treatment, the heavy metal ion (e.g., Cr^{3+}, Cu^{2+}, Ni^{2+}, and Zn^{2+}) leaching concentrations in EMR and RM were above the limit concentrations stated in Chinese standard GB5085.3–2007 (Cr^{3+}: 15 mg·L^{-1}, Cu^{2+}: 100 mg·L^{-1}, Ni^{2+}: 5 mg·L^{-1}, and Zn^{2+}: 100 mg·L^{-1}). After the mutual treatment, the heavy metal ion (e.g., Cr^{3+}, Cu^{2+}, Ni^{2+}, and Zn^{2+}) leaching concentrations in the ER were reduced to 1.45 mg·L^{-1}, 0.099 mg·L^{-1}, 0.294 mg·L^{-1}, and 0.449 mg·L^{-1}, respectively, denoting values below the concentrations restricted in Chinese standard GB5085.3–2007. In other words, the mutual harmless treatment of the RM and the EMR can also provide a good heavy metal ion solidification in both solid wastes.

Conclusions

This study used two hazardous wastes, EMR and RM, to investigate their mutual harmless treatment method. The alkaline substances in RM had a good effect on the treatment of ammonia nitrogen and soluble manganese ions in EMR. The suitable treatment conditions are as follows: the mass ratio of EMR to RM is 1:1, the ratio of liquid to solid is 1.4, and the stirring time is 320 min. Under suitable treatment conditions, the removal ratio of ammonia nitrogen and the solidification ratio of manganese ions can reach 85.87 and 86.63%, respectively.

The mutual treatment processing of EMR and RM can be divided into two stages. Stage I is the rapid reaction stage of ammonia nitrogen, manganese ions ($(NH_4)_2$ $Mg(SO_4)_2$, $(NH_4)_2Mn(SO_4)_2$, $(NH_4)_2SO_4$), and soluble alkaline (NaOH, KOH, and Na_2CO_3) in the system. Ammonia nitrogen is converted into ammonia gas, and soluble manganese ions are converted into oxide forms (such as KMn_8O_{16}). Stage II is the slow reaction stage of residual ammonia nitrogen, manganese ion, and insoluble alkaline in the system. The insoluble alkali with a destroyed structure gradually dissolved out OH^- and continued to consume ammonia nitrogen and manganese ions. The mutual treatment of EMR and RM also converts the alkaline substances in RM into neutral salts (Na_2SO_4, $Mg_3O(CO_3)_2$). The purpose of removing alkaline substances in RM was achieved.

The kinetic process of EMR and RM treatment reaction is controlled by membrane diffusion mechanism and chemical reaction mechanism, and the corresponding mechanism function is $\ln(1-x)/3+(1-x)^{(-1/3)}-1=k_3t$. Among them, the dissolution process of ammonia nitrogen, soluble manganese ions and alkaline substances is controlled by membrane diffusion mechanism. The reaction of ammonia nitrogen, manganese ions and OH^- ions to produce ammonia and solidify manganese precipitation is controlled by a chemical reaction mechanism.

The mutual treatment of EMR and RM can solidify Cr^{3+}, Cu^{2+}, Ni^{2+}, Zn^{2+}, and other heavy metal ions in the system. The leaching concentration of heavy metal ions such as Cr^{3+}, Cu^{2+}, Ni^{2+}, and Zn^{2+} in the treated filter residue is considerably lower than the limit concentration in the Chinese standard GB5085.3–2007.

Acknowledgements This research was supported by the National Key R&D Program of China (grant no. 2018YFC1903503), the Guizhou Province Science and Technology Project Plan (grant nos. (2020)4Y014 and (2021)YB484), and the Guizhou University Introduced Talents Research Project Contract (grant no. (2019) 70).

Author contribution Jing Zhang: sample preparation for experiment. Experimental data analysis and writing manuscripts. Yu Zhang and Jing Zhang's postgraduate tutor and helping to revise the manuscript. Rui Li, Weilong He, Junjie Yang, and Yu Wang are the members of the research group.

Funding Thanks to the National Key R&D Program for providing scientific research funds for this project.

Data availability Not applicable (the data used is presented in various tables and figures in this article).

Declarations

Ethics approval Not applicable.

Consent to participate Not applicable.

Consent for publication Not applicable.

Competing interests The authors declare no competing interests.

References

Chen H, Liu R, Liu Z et al (2016) Immobilization of Mn and NH 4+-N from electrolytic manganese residue waste[J]. Environ Sci Pollut Res 23:12352–12361

Chen Y, Long J, Chen S et al (2022) Multi-step purification of electrolytic manganese residue leachate using hydroxide sedimentation, struvite precipitation, chlorination and coagulation: advanced removal of manganese, ammonium, and phosphate[J]. Sci Total Environ 805:150237

Deng Y, Shu J, Lei T et al (2021) A green method for Mn2+ and NH4+-N removal in electrolytic manganese residue leachate by electric field and phosphorus ore flotation tailings[J]. Sep Purif Technol 270:118820

Distefano G, Spunta G, Colonna FP et al (1976) Transmission of electronic effects in substituted pyridine-N-oxides studied by ESCA[J]. Zeitschrift Für Naturforschung A 31(7):856–857

Dong J, Wang Y, Zhou M (2002) The vibrational spectrum of the MnO2− and MnO4− anions in solid argon[J]. Chem Phys Lett 364(5–6):511–516

Duan N, Fan W, Changbo Z et al (2010) Analysis of pollution materials generated from electrolytic manganese industries in China[J]. Resour Conserv Recycl 54(8):506–511

Duan J, Feng S, He W, et al (2021) TG-FTIR and Py-GC/MS combined with kinetic model to study the pyrolysis characteristics of electrolytic manganese residue[J]. J Anal Appl Pyrolysis 105203

He S, Jiang D, Hong M, et al (2021a) Hazard-free treatment and resource utilisation of electrolytic manganese residue: a review[J]. J Clean Prod 127224

He D, Shu J, Wang R et al (2021b) A critical review on approaches for electrolytic manganese residue treatment and disposal technology: reduction, pretreatment, and reuse[J]. J Hazard Mater 418:126235

Hu G, Lyu F, Khoso SA et al (2020) Staged leaching behavior of red mud during dealkalization with mild acid[J]. Hydrometallurgy 196:105422

Huang Y, Zhang Q (2022) Highly efficient removal of Cu (II) with modified electrolytic manganese residue as a novel adsorbent[J]. Arab J Sci Eng 47(5):6577–6589

Khairul MA, Zanganeh J, Moghtaderi B (2019) The composition, recycling and utilisation of Bayer red mud[J]. Resour Conserv Recycl 141:483–498

Klauber C, Gräfe M, Power G (2011) Bauxite residue issues: II. options for residue utilization[J]. Hydrometallurgy 108(1–2):11–32

Lan J, Dong Y, Xiang Y et al (2021) Selective recovery of manganese from electrolytic manganese residue by using water as extractant under mechanochemical ball grinding: mechanism and kinetics[J]. J Hazard Mater 415:125556

Li C, Zhong H, Wang S et al (2015) Removal of basic dye (methylene blue) from aqueous solution using zeolite synthesized from electrolytic manganese residue[J]. J Ind Eng Chem 23:344–352

Li L, Zhu Q, Man K et al (2017) Fluoride removal from liquid phase by Fe-Al-La trimetal hydroxides adsorbent prepared by iron and aluminum leaching from red mud[J]. J Mol Liq 237:164–172

Li Y, Huang H, Xu Z et al (2020) Mechanism study on manganese (II) removal from acid mine wastewater using red mud and its application to a lab-scale column[J]. J Clean Prod 253:119955

Li M, He Z, Zhong H et al (2021) Multi-walled carbon nanotubes facilitated Roxarsone elimination in SR-AOPs by accelerating electron transfer in modified electrolytic manganese residue and forming surface activated-complexes[J]. Water Res 200:117266

Liao M, Yin J, Ning C (2022) Research status and progress of Bayer red mud dealkalization [J]. Sichuan Metallurgy 44(02):9–13+35

Liu Z, Li H, Huang M et al (2017) Effects of cooling method on removal of sodium from active roasting red mud based on water leaching[J]. Hydrometallurgy 167:92–100

Liu X, Han Y, He F et al (2021) Characteristic, hazard and iron recovery technology of red mud-a critical review[J]. J Hazard Mater 420:126542

Liu S, Zhang H, Cheng J (2022) Study on oxalic acid leaching process and mechanism of ammonia nitrogen in electrolytic manganese slag [J]. Silicate Notif 41(02):715–724. https://doi.org/10.16552/j.cnki.issn1001-1625.2022.010

Liu G, Fan K, Li X (2006) Sodium silicon slag in alumina production [J]. Light Metals (02):13–17

Luo M, Qi X, Zhang Y et al (2017) Study on dealkalization and settling performance of red mud[J]. Environ Sci Pollut Res 24(2):1794–1802

Mishra S, Bal R, Dey RK (2021) Heterogeneous recyclable copper oxide supported on activated red mud as an efficient and stable catalyst for the one pot hydroxylation of benzene to phenol[J]. Molecular Catalysis 499:111310

Patil SV, Thorat BN (2022) Mechanical dewatering of red mud[J]. Sep Purif Technol 121157

Peng T, Xu L, Chen H (2010) Preparation and characterization of high specific surface area Mn3O4 from electrolytic manganese residue[J]. Cent Eur J Chem 8(5):1059–1068

Qian J, Hou P, Wang Z et al (2012) Crystallization characteristic of glass-ceramic made from electrolytic manganese residue[J]. J Wuhan Univ Technol-Mater Sci Ed 27(1):45–49

Shu J, Liu R, Liu Z et al (2016) Solidification/stabilization of electrolytic manganese residue using phosphate resource and low-grade MgO/CaO[J]. J Hazard Mater 317:267–274

Shu J, Liu R, Liu Z et al (2017) Leaching of manganese from electrolytic manganese residue by electro-reduction[J]. Environ Technol 38(16):2077–2084

Shu J, Liu R, Wu H et al (2018) Adsorption of methylene blue on modified electrolytic manganese residue: kinetics, isotherm, thermodynamics and mechanism analysis[J]. J Taiwan Inst Chem Eng 82:351–359

Shu J, Wu H, Chen M et al (2019) Fractional removal of manganese and ammonia nitrogen from electrolytic metal manganese residue leachate using carbonate and struvite precipitation[J]. Water Res 153:229–238

Shu J, Lin F, Chen M et al (2020a) An innovative method to enhance manganese and ammonia nitrogen leaching from electrolytic manganese residue by surfactant and anode iron plate[J]. Hydrometallurgy 193:105311

Shu J, Cai L, Zhao J et al (2020b) A low cost of phosphate-based binder for Mn2+ and NH4+-N simultaneous stabilization in electrolytic manganese residue[J]. Ecotoxicol Environ Saf 205:111317

Shu J, Zeng X, Sun D, et al (2021) Enhanced Mn^{2+} solidification and NH^{4+}-N removal from electrolytic manganese metal residue via surfactants[J]. Chinese J Chem Eng

Tian Y, Shu J, Chen M et al (2019) Manganese and ammonia nitrogen recovery from electrolytic manganese residue by electric field enhanced leaching[J]. J Clean Prod 236:117708

Umezawa Y, Reilley CN (1978) Effect of argon ion bombardment on metal complexes and oxides studied by x-ray photoelectron spectroscopy[J]. Anal Chem 50(9):1290–1295

Wang J, Peng B, Chai L et al (2013) Preparation of electrolytic manganese residue–ground granulated blastfurnace slag cement[J]. Powder Technol 241:12–18

Wang X, Zhang Y, Liu J et al (2018a) Dealkalization of red mud by carbide slag and flue gas[J]. CLEAN–Soil, Air, Water 46(3):1700634

Wang Y, Zhang T, Lyu G et al (2018b) Recovery of alkali and alumina from bauxite residue (red mud) and complete reuse of the treated residue[J]. J Clean Prod 188:456–465

Winkler D, Bidló A, Bolodár-Varga B et al (2018) Long-term ecological effects of the red mud disaster in Hungary: regeneration of red mud flooded areas in a contaminated industrial region[J]. Sci Total Environ 644:1292–1303

Yang C, Lv X, Tian X et al (2014) An investigation on the use of electrolytic manganese residue as filler in sulfur concrete[J]. Constr Build Mater 73:305–310

Zhang W, Cheng CY (2007) Manganese metallurgy review Part I: leaching of ores/secondary materials and recovery of electrolytic/chemical manganese dioxide[J]. Hydrometallurgy 89(3–4):137–159

Zhang G, Li S, Zhang X, Wang Z (2012) Study on the alkali elution process of Bayer red mud water [J]. J Qingdao Univ Technol 33(04):59–62

Zhang Y, Liu X, Xu Y et al (2020) Preparation of road base material by utilizing electrolytic manganese residue based on Si-Al structure: mechanical properties and Mn2+ stabilization/solidification characterization[J]. J Hazard Mater 390:122188

Zhou C, Wang J, Wang N (2013) Treating electrolytic manganese residue with alkaline additives for stabilizing manganese and removing ammonia[J]. Korean J Chem Eng 30(11):2037–2042